# Flexible three dimensional gear modelling

**Alberto Cardona**

*Computational Mechanics Laboratory - INTEC*
*Universidad Nacional del Litoral - CONICET*
*Güemes 3450, 3000 Santa Fe, Argentine*

ABSTRACT. *We present a formulation for describing flexible gear pairs in the three dimensional analysis of flexible mechanisms. The set of holonomic and no-holonomic constraint equations that defines the behavior of gears is developed. The formulation is capable of representing almost any kind of gears used in industry : spur gears, bevel gears, hypoid gears, racks, etc. All reaction forces due to gear engagement are accounted for. Teeth flexibility, clearance and mesh stiffness fluctuation are introduced in the model by relating deformation along the normal pressure line to the normal forces acting on teeth.*

RÉSUMÉ. *On présente une formulation pour décrire un couple d'engrenages flexibles en analyse tridimensionnelle de mécanismes flexibles. L'ensemble d'équations de restriction holonômes et non holonômes définissant le comportement d'engrenages est ici développé. La formulation peut représenter presque tous les types d'engrenages utilisés en industrie : engrenages droits, coniques, hypoïdales, crémaillères, etc. Toutes les forces de réaction engendrées par l'engrènement sont prises en compte. Les effets de flexibilité des dents, jeu et fluctuation de raideur sont introduits au modèle en considérant le rapport entre déformation le long de la ligne de pression normale et la force normale agissant sur les dents.*

KEY WORDS : *flexible mechanisms, finite rotations, nonlinear dynamics.*
MOTS-CLÉS : *mécanismes flexibles, rotations finies, dynamique non linéaire.*

Revue européenne des éléments finis. Volume 4 - n° 5-6/1995, pages 663 à 691

## 1. Introduction

Gears are devices of widespread use for the transmission of rotary motion from one shaft to another, which are present in almost every machine. A pair of gears with non intersecting and non parallel axes develops three dimensional gearing relative motion. All kinds of gears used in industry can be seen as particular cases of three dimensional gearing; e.g. spur gears, bevel gears, hypoid gears, worm gears, etc.

The literature on gears is vast and many classic texts treat them thoroughly (see for instance [JJ80] and references therein). Several studies on gear modeling have been published in recent years, most of them with the objective of improving the analysis capabilities to allow the design of smaller, lighter and quieter transmissions. An extensive review of recent literature on dynamic modeling of gears has been given in reference [HD88b]. Rama Mohana Rao and Muthuveerappan [RG93] evaluated root stresses for different positions of the contact line when it moves from the root to the tip in helical gear teeth using three dimensional finite elements. Özgüden et al [HNO91, SH93] developed non-linear mathematical models for dynamic analysis of a spur gear pair. They included shaft and bearing dynamics in the model, allowing to study the effect of lateral-torsional vibration coupling. Kahraman [AKa94a, AKa94b] developed a model to simulate the dynamic behavior of a single-stage planetary gear train with helical gears. The formulation allows to model planetary gear sets with any number of planets. The model was used to describe the effects of the planet mesh phasing on the dynamic behavior [AKa94a] and to predict the effect of manufacturing and assembly errors, and of tooth separations and mesh stiffness fluctuations on the load sharing between pinions [AKa94b]. Géradin and Robert [MG81] developed a general program to analyze torsional vibrations of gear trains. The model included effects as teeth flexibility, manufacturing errors (eccentricity), and stiffness fluctuation. The model of the gear train could be composed of parallel spur and helical gears, conical bevel gears and planetary systems. Xiao and Yang [DA89] used the concept of velocity screws and dual matrices to derive expressions to describe the kinematics of a pair of gears with non parallel and non intersecting axes.

In this paper we develop the equations of motion for representing three dimensional gearing, using the formulation of a general purpose code for flexible multibody analysis [SAM94, ACa89]. The gear is implemented as a particular flexible joint of the code, adding a new functionality to it. The code takes into account full three-dimensional motion, elasticity of members, damping, friction dissipation and many other effects. Code elements comprise a beam, membrane, rigid body, spring, hinge, cam, screw prismatic and cylindric joints within many others, allowing to make a highly realistic model of any machine. It can be linked to dynamic analysis finite element packages, incorporating thus easily arbitrary finite element models of elastic subsystems –either fixed or movable– to the numerical model of the mechanism.

This new joint is described by two physical nodes : one at the center of each wheel. Each node can be connected in turn to the other members of the mechanism. The formulation developed for the gear pair is general enough to represent almost every kind of gears used in industry : spur gears, helical gears, conical gears, internal gear and pinion, worm gears, hypoid gears, etc. This formulation generalizes a previously developed one [ACa95], by including the effects of gear teeth flexibility with fluctuating stiffness and backlash which were neglected before. We follow the method of Özgüden and Houser [HD88a] to include the excitation effect of mesh stiffness variation : it is considered as an internal excitation in the form of loaded static transmission error. This error can be calculated theoretically [MD86] or can be measured experimentally.

All components of contact forces induced by the gear pair are taken into account : tangential, radial and thrust forces. These forces are appropriately transmitted to the element nodes and to the other members of the mechanism. Friction forces are taken into account whenever appropriate (e.g. worm gearing). They are a function of the transmitted force, and of a friction coefficient. The friction coefficient varies with the instantaneous value of sliding velocity between worm and gear. Gear trains and planetary systems can be easily represented by superposing several gear pairs in the mechanism model.

The formulation developed for the gear pair is general enough to represent almost every kind of gears used in industry : spur gears, helical gears, conical gears, internal gear and pinion, worm gears, hypoid gears, etc. All components of contact forces induced by the gear pair are taken into account : tangential, radial and thrust forces. These forces are appropriately transmitted to the element nodes and to the other members of the mechanism. Friction forces are taken into account whenever appropriate (e.g. worm gearing). They are a function of the transmitted force, and of a friction coefficient. The friction coefficient varies with the instantaneous value of sliding velocity between worm and gear. Gear trains and planetary systems can be easily represented by superposing several gear pairs in the mechanism model.

We remark that most works in the literature limit the analysis to a particular gear pair configuration : e.g. spur gear pairs accounting for some components of flexibility in the system. In our formulation, we give a unified single treatment for any gear pair kind and combination. The resulting code allows to analyze almost any situation. The analyst can choose, by using the elements family, which effects are to be accounted for in the model.

In this paper we describe the formulation of the flexible gear pair composed by two wheels. We have tried to emphasize aspects concerning the inclusion of flexibility into the model. The formulation of rack and gear systems has been omitted for conciseness, as well as the formulation of friction forces between gears. Details regarding these two latter aspects are given in reference [ACa95]. Several examples of application are shown, illustrating the generality and power of the approach.

## 2. Formulation of the constrained dynamics problem

The equations of motion for a dynamic system subjected to holonomic constraints $\mathbf{\Phi}$ can be stated in the form [ACa89, AMD91] :

$$\begin{cases} \frac{d}{dt}\left(\frac{\partial \mathcal{L}}{\partial \dot{\mathbf{q}}}\right) - \frac{\partial \mathcal{L}}{\partial \mathbf{q}} = \mathbf{Q} + \mathbf{Q}' \\ k\mathbf{\Phi}(\dot{\mathbf{q}}, \mathbf{q}, t) = \mathbf{0} \end{cases} \tag{1}$$

where an augmented Lagrangian approach is followed, $\mathcal{L}$ is the Lagrangian of the unconstrained dynamic system, $\mathbf{q}$ and $\dot{\mathbf{q}}$ are the generalized displacements and velocities of the dynamic system, and $\mathbf{Q}$ are the non-conservative forces acting on the system (they include, for instance, the friction and damping forces). The constraint forces $\mathbf{Q}'$, which can be thought of as the generalized forces that oblige the system to verify the imposed constraints, are

$$\mathbf{Q}' = (k\lambda_i - p\Phi_i)\frac{\partial \Phi_i}{\partial \mathbf{q}} \tag{2}$$

where $k$ and $p$ are the scale and the penalty factors, respectively. The penalty term does not modify the stationary properties of the original Lagrangian function –i.e. the value of the solution is not altered– but adds some positive curvature in the range space of $\frac{\partial \Phi_i}{\partial \mathbf{q}}$, with a significant improvement of convergence of the iterative scheme [ACa89, AMD91]. The values of $k$ and $p$ should be chosen so as to adequately balance the equations : a mean value of the stiffness of the mechanism usually represents an appropriate choice for them.

Equations (1) form a system of nonlinear differential-algebraic equations. The solution is advanced step-by-step using a time integration scheme (in particular, we used the Hilber-Hughes-Taylor method, see [AM89, AM94] for details). At each time step, a system of nonlinear algebraic equations has to be solved. In order to solve this system, we use the Newton method. The contribution of the holonomic constraints to the iteration matrix is obtained by differentiating constraint forces and constraints with respect to the generalized displacements vector :

$$\mathbf{S} = \begin{bmatrix} p\mathbf{B}\mathbf{B}^T & -k\mathbf{B} \\ -k\mathbf{B}^T & \mathbf{0} \end{bmatrix} \tag{3}$$

where second order derivatives of constraints have been neglected (experience has shown that neglecting these terms does not alter significantly the convergence rate of the algorithm [ACa89, AMD91]).

## 3. Kinematics of the joint

### *3.1. Basic definitions*

We will consider a joint formed by two geared wheels with centers $A$ and $B$. In this section we define some basic elements that will be used to express the kinematics relations of the joint.

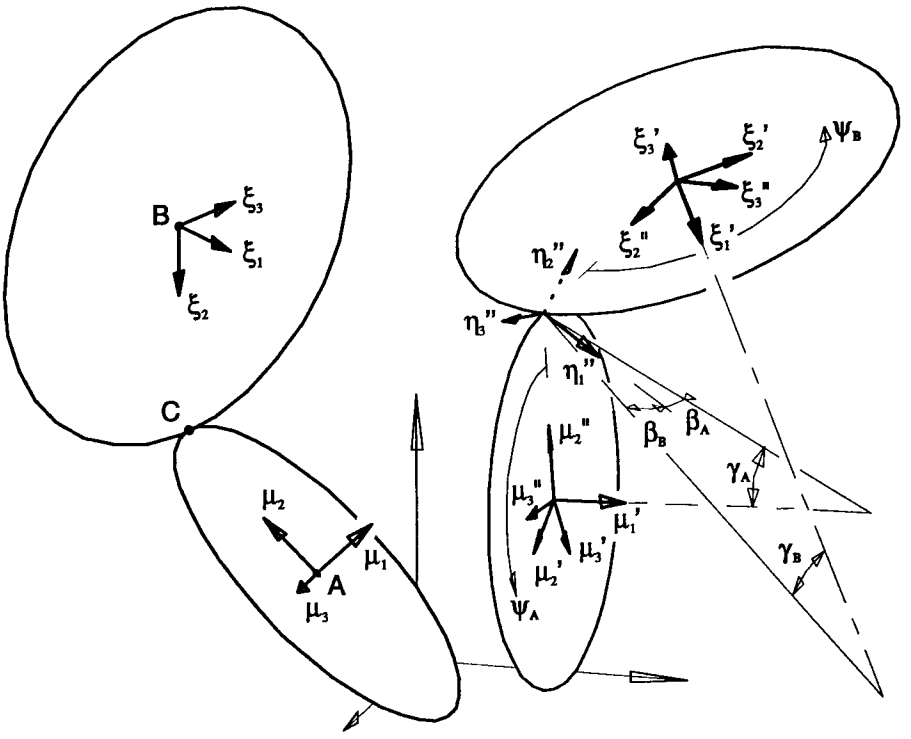


Figure 1: *Gear pair kinematics*

The position of each wheel center in the inertial frame is given by $\mathbf{x}_A$ and $\mathbf{x}_B$. Let us define one triad of unit orthogonal vectors at each wheel center at the reference configuration :

- $\{\boldsymbol{\mu}_1, \boldsymbol{\mu}_2, \boldsymbol{\mu}_3\}$ attached to the first wheel, with origin at its center $A$;
- $\{\boldsymbol{\xi}_1, \boldsymbol{\xi}_2, \boldsymbol{\xi}_3\}$ attached to the second wheel, with origin at node $B$.

Both triads are dextrorsum and have their first vector perpendicularly oriented to the wheel plane and their second vector oriented towards the contact point between wheels (see figure 1). Explicit expressions for vectors $\boldsymbol{\mu}_2, \boldsymbol{\mu}_3, \boldsymbol{\xi}_2, \boldsymbol{\xi}_3$, obtained according these guidelines, are given afterwards in section (3.2).

**Remark :** The distance between centers at the current configuration as well as the relative orientation of both wheels, should be kept constant by some external means (e.g. a frame) to maintain the correct engagement. The present formulation of the joint does not take into account variations in the centers distance to correct the transmission relation.

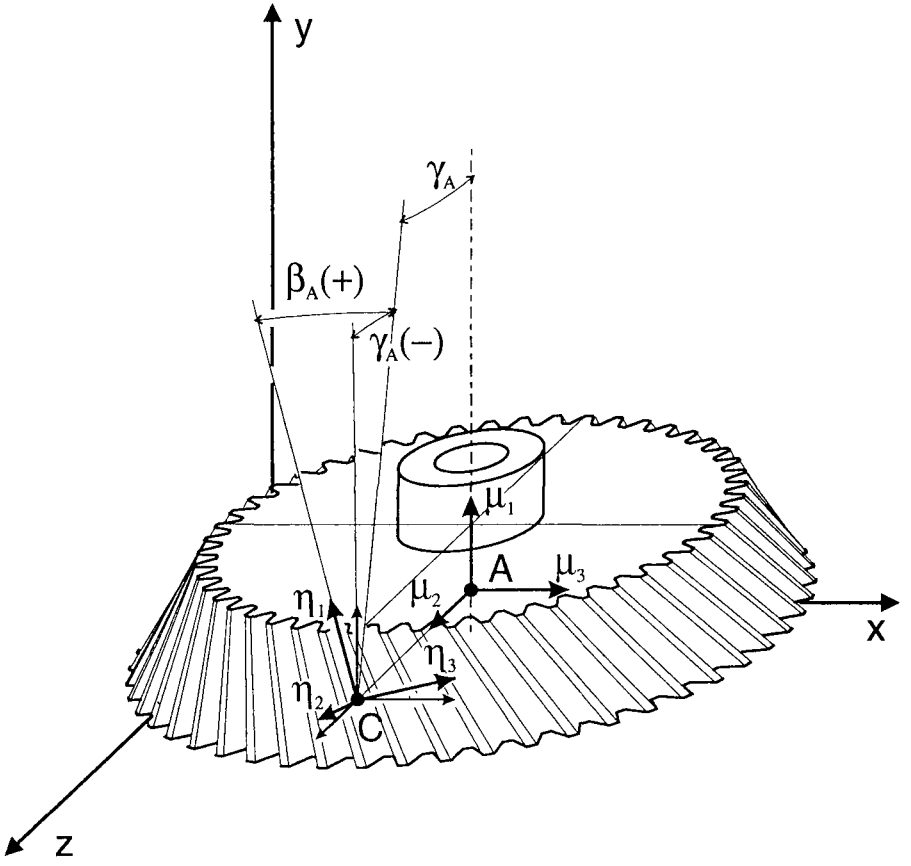


Figure 2: *Sign conventions for cone and helix angles*

The orientation of both material triads at the current configuration is obtained applying the rotation operator of each wheel to the vectors at the reference configuration :

$$\boldsymbol{\mu}_i' = \mathbf{R}_A \boldsymbol{\mu}_i \qquad \boldsymbol{\xi}_i' = \mathbf{R}_B \boldsymbol{\xi}_i \qquad i = 1,3 \tag{4}$$

$\mathbf{R}_A, \mathbf{R}_B$ are the rotation matrices at nodes $A, B$, which are related to the rotation vectors $\boldsymbol{\Theta}_A, \boldsymbol{\Theta}_B$ through the exponential forms $\exp(\widetilde{\boldsymbol{\Theta}}_A), \exp(\widetilde{\boldsymbol{\Theta}}_B)$ [ACa89, AM88].

We define a second pair of unit triads at the current configuration. These triads are attached to the supporting frame of the gear pair. They are built following the same rule we used to get the reference triads $\{\boldsymbol{\mu}_1, \boldsymbol{\mu}_2, \boldsymbol{\mu}_3\}$ and $\{\boldsymbol{\xi}_1, \boldsymbol{\xi}_2, \boldsymbol{\xi}_3\}$. I.e., vectors $\boldsymbol{\mu}_1''$ and $\boldsymbol{\xi}_1''$ are normal to each wheel :

$$\boldsymbol{\mu}_1'' = \boldsymbol{\mu}_1' = \mathbf{R}_A \boldsymbol{\mu}_1 \qquad \boldsymbol{\xi}_1'' = \boldsymbol{\xi}_1' = \mathbf{R}_B \boldsymbol{\xi}_1 \tag{5}$$

while vectors $\boldsymbol{\mu}_2'', \boldsymbol{\xi}_2''$ point towards the contact point and vectors $\boldsymbol{\mu}_3'', \boldsymbol{\xi}_3''$ complete a dextrorsum triad.

We also define a triad of unit vectors $\{\boldsymbol{\eta}_1'', \boldsymbol{\eta}_2'', \boldsymbol{\eta}_3''\}$, which are oriented along the teeth in contact at the current configuration : $\boldsymbol{\eta}_1''$ is parallel to the tooth baseline; $\boldsymbol{\eta}_2''$ points along the tooth vertical line, from the first wheel to the second one; finally, $\boldsymbol{\eta}_3''$ is normal to the tooth midplane.

The triad $\{\boldsymbol{\eta}_i''\}$ is related to $\{\boldsymbol{\mu}_i''\}$ through the angles of cone $\gamma_A$ and helix $\beta_A$, as shown in figure 1 :

$$[\boldsymbol{\eta}_1''^A \quad \boldsymbol{\eta}_2''^A \quad \boldsymbol{\eta}_3''^A] = [\boldsymbol{\mu}_1'' \quad \boldsymbol{\mu}_2'' \quad \boldsymbol{\mu}_3''] \, \mathbf{Y}_A \tag{6}$$

The explicit expression of the orthogonal matrix $\mathbf{Y}_A$ follows :

$$\mathbf{Y}_A = \mathbf{Y}(\gamma_A, \beta_A) = \begin{bmatrix} \cos\gamma_A \cos\beta_A & -\sin\gamma_A & \cos\gamma_A \sin\beta_A \\ \sin\gamma_A \cos\beta_A & \cos\gamma_A & \sin\gamma_A \sin\beta_A \\ -\sin\beta_A & 0 & \cos\beta_A \end{bmatrix} \tag{7}$$

The sign conventions for the cone and helix angles are described in figure 2.

**Remark :** The superscript $A$ in equation (6) is used to emphasize that vectors $\boldsymbol{\eta}_i''^A$ are here computed in terms of kinematics variables at wheel $A$ only.

**Remark :** Note that internal gears are represented by selecting $\gamma_A = 180\,\text{deg}$.

Similar relations hold between $\{\boldsymbol{\eta}_i''\}$ and $\{\boldsymbol{\xi}_i''\}$ through the angles $\gamma_B$ and $\beta_B$, with the only difference that signs are changed to match the condition of gear engagement (note that the triad $\boldsymbol{\eta}_i''$ has been defined as pointing from the first wheel to the second one) :

$$[\boldsymbol{\eta}_1''^B \quad \boldsymbol{\eta}_2''^B \quad \boldsymbol{\eta}_3''^B] = [\boldsymbol{\xi}_1'' \quad \boldsymbol{\xi}_2'' \quad \boldsymbol{\xi}_3''] \underbrace{\mathbf{Y}(\gamma_B, \beta_B) \begin{bmatrix} 1 & 0 & 0 \\ 0 & -1 & 0 \\ 0 & 0 & -1 \end{bmatrix}}_{\mathbf{Y}_B} \tag{8}$$

We get the relation between triads $\{\boldsymbol{\mu}_i''\}$ and $\{\boldsymbol{\xi}_i''\}$ at engagement by equating equations (6) and (8) :

$$\begin{aligned} [\boldsymbol{\xi}_1'' \quad \boldsymbol{\xi}_2'' \quad \boldsymbol{\xi}_3''] &= [\boldsymbol{\mu}_1'' \quad \boldsymbol{\mu}_2'' \quad \boldsymbol{\mu}_3''] \, \mathbf{Y}_A \mathbf{Y}_B^T \\ &= [\boldsymbol{\mu}_1'' \quad \boldsymbol{\mu}_2'' \quad \boldsymbol{\mu}_3''] \, \mathbf{Z}(\gamma_A, \beta_A, \gamma_B, \beta_B) \end{aligned} \tag{9}$$

**Remark :** It can be easily shown that $\mathbf{Z}$ is in fact a function of the three independent parameters $(\gamma_A, \gamma_B, \beta_A - \beta_B)$.

### 3.2. *Explicit expressions of vectors $\mu_2, \mu_3, \xi_2, \xi_3$ at the reference configuration*

First, we determine the position of the contact point $\mathbf{x}_C$. It can be computed either in terms of kinematics variables at wheel $A$ or at wheel $B$ :

$$\begin{array}{rcl} \mathbf{x}_C^A & = & \mathbf{x}_A + \mathbf{r}_A \; = \; \mathbf{x}_A + \boldsymbol{\mu}_2'' r_A \\ \mathbf{x}_C^B & = & \mathbf{x}_B + \mathbf{r}_B \; = \; \mathbf{x}_B + \boldsymbol{\xi}_2'' r_B \end{array} \tag{10}$$

where $\mathbf{r}_A, \mathbf{r}_B$ are the radius vectors from the wheels centers to the contact point

$$\mathbf{r}_A \; = \; r_A \boldsymbol{\mu}_2'' \qquad\qquad \mathbf{r}_B \; = \; r_B \boldsymbol{\xi}_2'' \tag{11}$$

Using equation (9), we compute vector $\boldsymbol{\xi}_2''$ in terms of vectors $\boldsymbol{\mu}_i''$ :

$$\boldsymbol{\xi}_2'' \; = \; \sum_{i=1,3} \boldsymbol{\mu}_i'' Z_{i,2} \tag{12}$$

Then, we can write the equation for the relative position of $\mathbf{x}_B$ with respect to $\mathbf{x}_A$ as indicated below :

$$\mathbf{x}_{AB} \; = \; \mathbf{x}_B - \mathbf{x}_A \; = \; \boldsymbol{\mu}_2'' r_A - \sum_{i=1,3} \boldsymbol{\mu}_i'' Z_{i,2}\, r_B \tag{13}$$

Noting that $\boldsymbol{\mu}_3'' = \boldsymbol{\mu}_1'' \times \boldsymbol{\mu}_2''$, and since $\boldsymbol{\mu}_i = \boldsymbol{\mu}_i''$ at the reference configuration, we obtain the system of equations :

$$[(r_B Z_{2,2} - r_A)\mathbf{1} + Z_{3,2}\, r_B \widetilde{\boldsymbol{\mu}}_1]\; \boldsymbol{\mu}_2 \; = \; -\mathbf{x}_{AB} - r_B Z_{1,2}\; \boldsymbol{\mu}_1 \tag{14}$$

We get the expression of $\boldsymbol{\mu}_2$ by solving this system :

$$\boldsymbol{\mu}_2 \; = \; c_1 \mathbf{x}_{AB} + c_2 \boldsymbol{\mu}_1 + c_3 \boldsymbol{\mu}_1 \times \mathbf{x}_{AB} \tag{15}$$

where constants $(c_1, c_2, c_3)$ are defined as follows :

$$c \; = \; (r_A - Z_{2,2}\, r_B)^2 - Z_{3,2}^2\, r_B^2 \qquad \begin{array}{rcl} c_1 & = & (r_A - Z_{2,2}\, r_B)/c \\ c_2 & = & (r_A - Z_{2,2}\, r_B) Z_{1,2}\, r_B / c \\ c_3 & = & Z_{3,2}\, r_B / c \end{array} \tag{16}$$

The third vector $\boldsymbol{\mu}_3$ is then computed :

$$\boldsymbol{\mu}_3 \; = \; \boldsymbol{\mu}_1 \times \boldsymbol{\mu}_2 \; = \; c_1\, \boldsymbol{\mu}_1 \times \mathbf{x}_{AB} - c_3\, [\mathbf{1} - \boldsymbol{\mu}_1 \otimes \boldsymbol{\mu}_1] \mathbf{x}_{AB} \tag{17}$$

Vectors $\boldsymbol{\xi}_2, \boldsymbol{\xi}_3$ are afterwards computed using equation (9) : $[\boldsymbol{\xi}_1 \quad \boldsymbol{\xi}_2 \quad \boldsymbol{\xi}_3] = [\boldsymbol{\mu}_1 \quad \boldsymbol{\mu}_2 \quad \boldsymbol{\mu}_3]\, \mathbf{Z}$.

> **Remark :** It can be shown numerically that $c \neq 0$ for $r_A \geq r_B$. Therefore, we ask this condition be satisfied to assure the system of equations (14) is solvable.

### 3.3. *Degrees of freedom of the joint*

The pair is formed by two rigid bodies (the two wheels) related by one kinematics constraint that links the rotations of both wheels about their respective normal axes. Fifteen kinematics variables are used to describe the joint, grouped together into the generalized coordinates vector $\mathbf{q}$ :

$$\mathbf{q} = \langle \mathbf{x}_A^T \quad \boldsymbol{\Theta}_A^T \quad \mathbf{x}_B^T \quad \boldsymbol{\Theta}_B^T \quad \psi_A \quad \psi_B \quad u_m \rangle \tag{18}$$

Recall $\mathbf{x}_A, \mathbf{x}_B$ give the position and $\boldsymbol{\Theta}_A, \boldsymbol{\Theta}_B$ give the rotation vector of each wheel center. The scalar value $u_m$ measures the deformation of the gear mesh in the hoop direction. This value is in fact a combined measure resulting from tooth deformation at both wheels and clearance between teeth. Finally, the angular displacements $\psi_A, \psi_B$ measure the relative rotation of each wheel in the local frame, resulting in the following relations between quoted and doubly-quoted frames :

$$\begin{aligned} \boldsymbol{\mu}_2'' &= \boldsymbol{\mu}_2' \cos\psi_A - \boldsymbol{\mu}_3' \sin\psi_A & \qquad \boldsymbol{\mu}_3'' &= \boldsymbol{\mu}_2' \sin\psi_A + \boldsymbol{\mu}_3' \cos\psi_A \\ \boldsymbol{\xi}_2'' &= \boldsymbol{\xi}_2' \cos\psi_B - \boldsymbol{\xi}_3' \sin\psi_B & \qquad \boldsymbol{\xi}_3'' &= \boldsymbol{\xi}_2' \sin\psi_B + \boldsymbol{\xi}_3' \cos\psi_B \end{aligned} \tag{19}$$

These relations can be written in matrix form :

$$\begin{aligned} [\boldsymbol{\mu}_1'' \quad \boldsymbol{\mu}_2'' \quad \boldsymbol{\mu}_3''] &= [\boldsymbol{\mu}_1' \quad \boldsymbol{\mu}_2' \quad \boldsymbol{\mu}_3'] \, \mathbf{R}(\mathbf{e}_1, \psi_A) \\ [\boldsymbol{\xi}_1'' \quad \boldsymbol{\xi}_2'' \quad \boldsymbol{\xi}_3''] &= [\boldsymbol{\xi}_1' \quad \boldsymbol{\xi}_2' \quad \boldsymbol{\xi}_3'] \, \mathbf{R}(\mathbf{e}_1, \psi_B) \end{aligned} \tag{20}$$

with

$$\mathbf{R}(\mathbf{e}_1, \psi) = \begin{bmatrix} 1 & 0 & 0 \\ 0 & \cos\psi & -\sin\psi \\ 0 & \sin\psi & \cos\psi \end{bmatrix}$$

The joint has twelve physical degrees of freedom : the six components of rigid body motion at each wheel plus the elastic deformation of the mesh minus the rotation constraint between wheels. Therefore, the dimension of the vector of kinematics variables $\mathbf{q}$ exceeds by three the number of physical degrees of freedom of the joint, and we have to impose a total of three constraints. One constraint is the kinematics relation resulting from teeth contact, and two additional ones fix the value of the relative angular displacements $\psi_A, \psi_B$. The set of constraints is described in the next section. Three Lagrange multipliers –conjugated to these constraints– are added to the generalized coordinates $\mathbf{q}$ to form the vector of unknowns of the joint.

### 3.4. *Variations of vectors* $\boldsymbol{\mu}_i'', \boldsymbol{\xi}_i'', \boldsymbol{\eta}_i''$

By taking variations in equation (10), we can write :

$$\begin{aligned} \delta\mathbf{x}_C^A &= \delta\mathbf{x}_A + \delta\boldsymbol{\mu}_2'' \, r_A \\ \delta\mathbf{x}_C^B &= \delta\mathbf{x}_B + \delta\boldsymbol{\xi}_2'' \, r_B \end{aligned} \tag{21}$$

The variation of vector $\boldsymbol{\mu}_2''$ is computed using equation (19) :

$$\begin{aligned} \delta\boldsymbol{\mu}_2'' &= \delta\boldsymbol{\mu}_2' \cos\psi_A - \delta\boldsymbol{\mu}_3' \sin\psi_A - \boldsymbol{\mu}_2' \sin\psi_A \delta\psi_A - \boldsymbol{\mu}_3' \cos\psi_A \delta\psi_A \\ &= (\mathbf{R}_A \delta\boldsymbol{\Theta}_A) \times \boldsymbol{\mu}_2'' - \boldsymbol{\mu}_3'' \, \delta\psi_A \end{aligned} \tag{22}$$

For the rest of the doubly-quoted vectors we get, in the same fashion

$$\begin{array}{rcl} \delta\boldsymbol{\mu}_3'' & = & (\mathbf{R}_A\delta\boldsymbol{\Theta}_A)\times\boldsymbol{\mu}_3'' + \boldsymbol{\mu}_2''\,\delta\psi_A \\ \delta\boldsymbol{\xi}_2'' & = & (\mathbf{R}_B\delta\boldsymbol{\Theta}_B)\times\boldsymbol{\xi}_2'' - \boldsymbol{\xi}_3''\,\delta\psi_B \\ \delta\boldsymbol{\xi}_3'' & = & (\mathbf{R}_B\delta\boldsymbol{\Theta}_B)\times\boldsymbol{\xi}_3'' + \boldsymbol{\xi}_2''\,\delta\psi_B \end{array} \tag{23}$$

After replacing the variations of $\boldsymbol{\mu}_2'', \boldsymbol{\xi}_2''$ into equation (21), we can compute the variations of position of the contact point computed in terms of kinematics variables at wheel $A$ or at wheel $B$ :

$$\begin{array}{rcl} \delta\mathbf{x}_C^A & = & \delta\mathbf{x}_A + (\mathbf{R}_A\delta\boldsymbol{\Theta}_A)\times\boldsymbol{\mu}_2''r_A - \boldsymbol{\mu}_3''\delta\psi_A r_A \\ \delta\mathbf{x}_C^B & = & \delta\mathbf{x}_B + (\mathbf{R}_B\delta\boldsymbol{\Theta}_B)\times\boldsymbol{\xi}_2''r_B - \boldsymbol{\xi}_3''\delta\psi_B r_B \end{array} \tag{24}$$

Equations (22,23) can be written in matrix form

$$\begin{array}{rcl} [\delta\boldsymbol{\mu}_1'' \quad \delta\boldsymbol{\mu}_2'' \quad \delta\boldsymbol{\mu}_3''] & = & [\widetilde{\mathbf{R}_A\delta\boldsymbol{\Theta}_A}]\,[\boldsymbol{\mu}_1'' \quad \boldsymbol{\mu}_2'' \quad \boldsymbol{\mu}_3''] + \delta\psi_A\,[\mathbf{0} \quad -\boldsymbol{\mu}_3'' \quad \boldsymbol{\mu}_2''] \\ [\delta\boldsymbol{\xi}_1'' \quad \delta\boldsymbol{\xi}_2'' \quad \delta\boldsymbol{\xi}_3''] & = & [\widetilde{\mathbf{R}_B\delta\boldsymbol{\Theta}_B}]\,[\boldsymbol{\xi}_1'' \quad \boldsymbol{\xi}_2'' \quad \boldsymbol{\xi}_3''] + \delta\psi_B\,[\mathbf{0} \quad -\boldsymbol{\xi}_3'' \quad \boldsymbol{\xi}_2''] \end{array} \tag{25}$$

Finally, using equations (6-8) we establish the expressions for the variations of vectors $\boldsymbol{\eta}_i''^A, \boldsymbol{\eta}_i''^B$ :

$$\begin{array}{rcl} [\delta\boldsymbol{\eta}_1''^A \quad \delta\boldsymbol{\eta}_2''^A \quad \delta\boldsymbol{\eta}_3''^A] & = & [\widetilde{\mathbf{R}_A\delta\boldsymbol{\Theta}_A}]\,[\boldsymbol{\eta}_1''^A \quad \boldsymbol{\eta}_2''^A \quad \boldsymbol{\eta}_3''^A] \\ & & + \delta\psi_A\,[\mathbf{0} \quad -\boldsymbol{\mu}_3'' \quad \boldsymbol{\mu}_2'']\,\mathbf{Y}_A \\ [\delta\boldsymbol{\eta}_1''^B \quad \delta\boldsymbol{\eta}_2''^B \quad \delta\boldsymbol{\eta}_3''^B] & = & [\widetilde{\mathbf{R}_B\delta\boldsymbol{\Theta}_B}]\,[\boldsymbol{\eta}_1''^B \quad \boldsymbol{\eta}_2''^B \quad \boldsymbol{\eta}_3''^B] \\ & & + \delta\psi_B\,[\mathbf{0} \quad -\boldsymbol{\xi}_3'' \quad \boldsymbol{\xi}_2'']\,\mathbf{Y}_B \end{array} \tag{26}$$

## 4. Computation of the constraint forces

Three constraints are needed to fully determine the joint kinematics variables. The first equation of constraint gives the kinematics relation between angular displacements of both wheels :

$$\phi_1 \;=\; (-\psi_A z_A + \psi_B z_B)\,\frac{m_n\cos\alpha_n}{2} + u_m\cos\alpha_n \;=\; 0 \tag{27}$$

where $m_n$ is the normal module of the gear teeth, $\alpha_n$ the pressure angle in the normal plane, and $z_A$ and $z_B$ are the numbers of teeth at each wheel. It can be shown easily that by formulating the constraint in this way, the conjugated Lagrange multiplier –scaled by factor $k$– has the physical meaning of normal contact force : $\mathcal{F} = k\lambda_1$.

The second constraint represents the hoop contact constraint produced by engagement between teeth :

$$\phi_2 \;=\; (\mathbf{x}_C^A - \mathbf{x}_C^B)\cdot\boldsymbol{\eta}_3''^A \;=\; 0 \tag{28}$$

where $\mathbf{x}_C^A, \mathbf{x}_C^B$ give the position of the contact point computed on wheel $A$ and $B$, respectively.

The third constraint expresses that the triad $\boldsymbol{\eta}_i''$ is unique, when computed in terms of kinematics variables of either wheel :

$$\phi_3 \;=\; \boldsymbol{\eta}_2''^{A} \cdot \boldsymbol{\eta}_3''^{B} \;=\; 0 \tag{29}$$

The variation of $\phi_1$ is simply written

$$\delta\phi_1 \;=\; \delta\mathbf{q} \cdot \frac{\partial \phi_1}{\partial \mathbf{q}} \;=\; \left\{ \begin{array}{c} \delta\mathbf{x}_A \\ \delta\boldsymbol{\Theta}_A \\ \delta\mathbf{x}_B \\ \delta\boldsymbol{\Theta}_B \\ \delta\psi_A \\ \delta\psi_B \\ \delta u_m \end{array} \right\} \cdot \left\{ \begin{array}{c} \mathbf{0} \\ \mathbf{0} \\ \mathbf{0} \\ \mathbf{0} \\ -\frac{1}{2} z_A m_n \cos\alpha_n \\ \frac{1}{2} z_B m_n \cos\alpha_n \\ \cos\alpha_n \end{array} \right\} \tag{30}$$

The variation of the second constraint can be written in the form :

$$\delta\phi_2 \;=\; (\delta\mathbf{x}_C^A - \delta\mathbf{x}_C^B) \cdot \boldsymbol{\eta}_3''^{A} \;+\; \delta\boldsymbol{\eta}_3''^{A} \cdot (\mathbf{x}_C^A - \mathbf{x}_C^B) \tag{31}$$

Using equations (24) and (26), we get :

$$\delta\phi_2 \;=\; \delta\mathbf{q} \cdot \frac{\partial \phi_2}{\partial \mathbf{q}} \;=\; \left\{ \begin{array}{c} \delta\mathbf{x}_A \\ \delta\boldsymbol{\Theta}_A \\ \delta\mathbf{x}_B \\ \delta\boldsymbol{\Theta}_B \\ \delta\psi_A \\ \delta\psi_B \\ \delta u_m \end{array} \right\} \cdot \left\{ \begin{array}{c} \boldsymbol{\eta}_3''^{A} \\ \mathbf{R}_A^T(\boldsymbol{\eta}_3''^{A} \times (\mathbf{x}_A - \mathbf{x}_C^B)) \\ -\boldsymbol{\eta}_3''^{A} \\ \mathbf{R}_B^T(\boldsymbol{\eta}_3''^{A} \times \mathbf{r}_B) \\ (Y_{A\,3,3}\,\boldsymbol{\mu}_2'' - Y_{A\,2,3}\,\boldsymbol{\mu}_3'') \cdot (\mathbf{x}_A - \mathbf{x}_C^B) \\ r_B\,\boldsymbol{\xi}_3'' \cdot \boldsymbol{\eta}_3''^{A} \\ 0 \end{array} \right\} \tag{32}$$

Variations of the third constraint are next computed

$$\delta\phi_3 \;=\; \boldsymbol{\eta}_2''^{A} \cdot \delta\boldsymbol{\eta}_3''^{B} + \boldsymbol{\eta}_3''^{B} \cdot \delta\boldsymbol{\eta}_2''^{A} \tag{33}$$

giving

$$\delta\phi_3 \;=\; \delta\mathbf{q} \cdot \frac{\partial \phi_3}{\partial \mathbf{q}} \;=\; \left\{ \begin{array}{c} \delta\mathbf{x}_A \\ \delta\boldsymbol{\Theta}_A \\ \delta\mathbf{x}_B \\ \delta\boldsymbol{\Theta}_B \\ \delta\psi_A \\ \delta\psi_B \\ \delta u_m \end{array} \right\} \cdot \left\{ \begin{array}{c} \mathbf{0} \\ \mathbf{R}_A^T(\boldsymbol{\eta}_2''^{A} \times \boldsymbol{\eta}_3''^{B}) \\ \mathbf{0} \\ -\mathbf{R}_B^T(\boldsymbol{\eta}_2''^{A} \times \boldsymbol{\eta}_3''^{B}) \\ -Y_{A\,2,2}\,\boldsymbol{\mu}_3'' \cdot \boldsymbol{\eta}_3''^{B} \\ (Y_{B\,3,3}\,\boldsymbol{\xi}_2'' - Y_{B\,2,3}\,\boldsymbol{\xi}_3'') \cdot \boldsymbol{\eta}_2''^{A} \\ 0 \end{array} \right\} \tag{34}$$

Afterwards, by substituting equations (30), (32) and (34) into equation (2), we evaluate the vector of constraint forces $\mathbf{Q}'$ of the joint :

$$\mathbf{Q}' \;=\; \left[ \begin{array}{ccc} \frac{\partial \phi_1}{\partial \mathbf{q}} & \frac{\partial \phi_2}{\partial \mathbf{q}} & \frac{\partial \phi_3}{\partial \mathbf{q}} \end{array} \right] \left\{ \begin{array}{c} (k\lambda_1 - p\Phi_1) \\ (k\lambda_2 - p\Phi_2) \\ (k\lambda_3 - p\Phi_3) \end{array} \right\} \;=\; \mathbf{B}\,\{\, k\boldsymbol{\lambda} - p\boldsymbol{\Phi} \,\} \tag{35}$$

The expression for the stiffness contribution follows immediately from equation (3).

## 5. Mesh deformation and clearance

Gears are assumed to be rigid disks, and the tooth mesh stiffness is represented by a nonlinear spring and damper inserted along the instantaneous pressure line. Time variation of mesh stiffness and non-linear effects due to backlash are very important in predicting the dynamic response in gears. Following Özgüven et al [HNO91, SH93], the parametric excitation effect of mesh stiffness variation is included in the form of a displacement excitation representing the fundamental harmonic of the loaded static transmission error. Separation of teeth and backlash is also included in the model, using the same approach.

Mesh forces are derived from the elastic potential $\mathcal{V}_m$, defined as follows:

$$\mathcal{V}_m = \frac{1}{2} k_m [[u_m + x_{err}]]^2 \tag{36}$$

with

$$[[x]] = \begin{cases} x & x \geq 0 \\ 0 & -b < x < 0 \\ x + b & x \leq -b \end{cases}$$

Here, $k_m$ is the mesh stiffness, $x_{err}$ is the loaded transmission error and $b$ is the hoop backlash. The loaded transmission error comprises both the mesh errors and mesh stiffness variations. We assume this term is a function of the angular displacement at one gear, e.g. $\psi_A$.

Mesh forces are computed next by taking variations with respect to the generalized displacement terms, giving :

$$\delta \mathcal{V}_m = \begin{Bmatrix} \delta\psi_A \\ \delta u_m \end{Bmatrix} \cdot k_m [[u_m + x_{err}]] \begin{Bmatrix} x'_{err} \\ 1 \end{Bmatrix} \tag{37}$$

By further differentiation we compute the tangent stiffness contribution :

$$\delta \mathbf{q} \cdot \mathbf{S}_m \Delta \mathbf{q} = \begin{Bmatrix} \delta\psi_A \\ \delta u_m \end{Bmatrix} \cdot k_m \begin{bmatrix} {x'_{err}}^2 + [[u_m + x_{err}]] x''_{err} & x'_{err} \\ x'_{err} & 1 \end{bmatrix} \begin{Bmatrix} \Delta\psi_A \\ \Delta u_m \end{Bmatrix} \tag{38}$$

with $x'_{err} = \partial x_{err} / \partial \psi_A$.

For the purpose of making some parametric studies, we have used the following expression for the loaded transmission error :

$$x_{err}(\psi_A) = X \left(1 - \cos\left(z_A \psi_A\right)\right) \tag{39}$$

where a perturbation of amplitude $X$ and one tooth frequency of excitation is assumed.

Mesh damping is accounted for by adding a term $c_m \dot{u}_m$ to the internal forces. The damping coefficient $c_m$ varies with the contact ratio. It can approximately be given as a function of the mesh damping ratio $\xi$ :

$$c_m = 2\xi \sqrt{k_m m_e} \tag{40}$$

with $m_e$ is an equivalent mass that represents both gear inertias, and is defined as

$$m_e = \frac{I_A I_B}{I_A R_B^2 + I_B R_A^2}. \tag{41}$$

(see reference [HNO91]).

## 6. Radial component of the contact force

Contact between teeth is produced along the pressure line. The orientation of the pressure line varies with the sign of the transmitted torque, in such a way that the contact force can be seen as always trying to separate both wheels. The contact force lies in the plane $\{\boldsymbol{\eta}_2'', \boldsymbol{\eta}_3''\}$, normally oriented to the teeth in contact. Its magnitude $\mathcal{F}$ is equal to $k\lambda_1$ (the Lagrange multiplier conjugated to the first constraint $\phi_1$ times the scale factor $k$).

The hoop and axial components of the contact force –oriented along $\boldsymbol{\eta}_3''$– have been taken into account when formulating the holonomic constraint $\phi_2$. However, the radial component of the contact force is of non-holonomic nature and has to be added explicitly to the formulation as a non-conservative force.

The radial component of force acting on wheel $A$ at the contact point is

$$\mathbf{F} = -|\mathcal{F}| \sin\alpha_n \boldsymbol{\eta}_2'' = -k|\lambda_1| \sin\alpha_n \boldsymbol{\eta}_2'' \tag{42}$$

while the opposite force $-\mathbf{F}$ acts upon wheel $B$ at the same point. We remark that $\mathbf{F}$ can be expressed indistinctly in terms of variables at either wheel. We will note :

$$\begin{aligned} \mathbf{F}^A &= -k|\lambda_1| \sin\alpha_n \boldsymbol{\eta}_2''^A \\ \mathbf{F}^B &= -k|\lambda_1| \sin\alpha_n \boldsymbol{\eta}_2''^B \end{aligned} \tag{43}$$

and use one or the other expression when appropriate. The radial contact force is conjugated to the variations of position of the contact point $C$, resulting in the following virtual work expression :

$$\begin{aligned} \delta\mathcal{W} &= \delta\mathbf{x}_C^A \cdot \mathbf{F}^A - \delta\mathbf{x}_C^B \cdot \mathbf{F}^B \\ &= \delta\mathbf{x}_A \cdot \mathbf{F}^A + \delta\boldsymbol{\Theta}_A \cdot \mathbf{R}_A^T(\mathbf{r}_A \times \mathbf{F}^A) \\ &\quad - \delta\mathbf{x}_B \cdot \mathbf{F}^B - \delta\boldsymbol{\Theta}_B \cdot \mathbf{R}_B^T(\mathbf{r}_B \times \mathbf{F}^B) \end{aligned} \tag{44}$$

where we have used the identities : $\boldsymbol{\mu}_3'' \cdot \mathbf{F}^A = 0 \quad ; \quad \boldsymbol{\xi}_3'' \cdot \mathbf{F}^B = 0$. The vector of non-conservative forces $\mathbf{Q}$ of the gear pair is identified as formed by the conjugated components to the variations of the generalized coordinates of the joint :

$$\delta\mathcal{W} = \delta\mathbf{q} \cdot \mathbf{Q} = \begin{Bmatrix} \delta\mathbf{x}_A \\ \delta\boldsymbol{\Theta}_A \\ \delta\mathbf{x}_B \\ \delta\boldsymbol{\Theta}_B \\ \delta\psi_A \\ \delta\psi_B \\ \delta u_m \end{Bmatrix} \cdot \begin{Bmatrix} \mathbf{F}^A \\ \mathbf{R}_A^T(\mathbf{r}_A \times \mathbf{F}^A) \\ -\mathbf{F}^B \\ -\mathbf{R}_B^T(\mathbf{r}_B \times \mathbf{F}^B) \\ 0 \\ 0 \\ 0 \end{Bmatrix} \tag{45}$$

The contribution to tangent stiffness is obtained by differentiation of equation (45). We compute first the increment of the contact force $\mathbf{F}^A$ :

$$\begin{aligned}\Delta\mathbf{F}^A &= -k|\lambda_1|\sin\alpha_n\Delta\boldsymbol{\eta}_2''^A - \mathrm{sign}(\lambda_1)k\sin\alpha_n\boldsymbol{\eta}_2''^A\Delta\lambda_1 \\ &= k|\lambda_1|\sin\alpha_n\widetilde{\boldsymbol{\eta}}_2''^A\mathbf{R}_A^T\Delta\boldsymbol{\Theta}_A - \mathrm{sign}(\lambda_1)k\sin\alpha_n\boldsymbol{\eta}_2''^A\Delta\lambda_1 \\ &\quad + k|\lambda_1|\sin\alpha_n\left(-Y_{A\,2,2}\,\boldsymbol{\mu}_3'' + Y_{A\,3,2}\,\boldsymbol{\mu}_2''\right)\Delta\psi_A \\ &= -\widetilde{\mathbf{F}}^A\mathbf{R}_A^T\Delta\boldsymbol{\Theta}_A - c_A\boldsymbol{\mu}_3''\Delta\psi_A + (\mathbf{F}^A/\lambda_1)\Delta\lambda_1\end{aligned} \tag{46}$$

with

$$c_A = k|\lambda_1|\sin\alpha_n Y_{A\,2,2} \tag{47}$$

Similarly,

$$\Delta\mathbf{F}^B = -\widetilde{\mathbf{F}}^B\mathbf{R}_B^T\Delta\boldsymbol{\Theta}_B - c_B\boldsymbol{\xi}_3''\Delta\psi_B + (\mathbf{F}^B/\lambda_1)\Delta\lambda_1 \tag{48}$$

with

$$c_B = k|\lambda_1|\sin\alpha_n Y_{B\,2,2} \tag{49}$$

The increments of moments are computed next. First note that :

$$\begin{aligned}\Delta(\mathbf{R}_A^T\mathbf{r}_A) &= -r_A\mathbf{R}_A^T\boldsymbol{\mu}_3''\Delta\psi_A \\ \Delta(\mathbf{R}_A^T\mathbf{F}^A) &= \mathbf{R}_A^T(\mathbf{F}^A/\lambda_1)\Delta\lambda_1 - c_A\mathbf{R}_A^T\boldsymbol{\mu}_3''\Delta\psi_A\end{aligned} \tag{50}$$

Therefore :

$$\Delta(\mathbf{R}_A^T(\mathbf{r}_A\times\mathbf{F}^A)) = \mathbf{R}_A^T\widetilde{\mathbf{r}}_A(\mathbf{F}^A/\lambda_1)\Delta\lambda_1 + \mathbf{R}_A^T(r_A\widetilde{\mathbf{F}}^A - c_A\widetilde{\mathbf{r}}_A)\boldsymbol{\mu}_3''\Delta\psi_A \tag{51}$$

Also,

$$\Delta(\mathbf{R}_B^T(\mathbf{r}_B\times\mathbf{F}^B)) = \mathbf{R}_B^T\widetilde{\mathbf{r}}_B(\mathbf{F}^B/\lambda_1)\Delta\lambda_1 + \mathbf{R}_B^T(r_B\widetilde{\mathbf{F}}^B - c_B\widetilde{\mathbf{r}}_B)\boldsymbol{\xi}_3''\Delta\psi_B \tag{52}$$

Equations (46),(48),(51) and (52) give the contributions to the rows of the (non-symmetric) tangent stiffness matrix $\mathbf{S}$, such that :

$$\delta^2\mathcal{W} = \begin{Bmatrix}\delta\mathbf{q}\\ \delta\boldsymbol{\lambda}\end{Bmatrix}\cdot\begin{bmatrix}\mathbf{S}_{qq} & \mathbf{S}_{q\lambda}\\ \mathbf{S}_{\lambda q} & \mathbf{S}_{\lambda\lambda}\end{bmatrix}\begin{Bmatrix}\Delta\mathbf{q}\\ \Delta\boldsymbol{\lambda}\end{Bmatrix} \tag{53}$$

where :

$$\mathbf{S}_{qq} = \begin{bmatrix}\mathbf{0} & -\widetilde{\mathbf{F}}^A\mathbf{R}_A^T & \mathbf{0} & \mathbf{0} & -c_A\boldsymbol{\mu}_3'' & \mathbf{0} & \mathbf{0}\\ \mathbf{0} & \mathbf{0} & \mathbf{0} & \mathbf{0} & \mathbf{X}_A\boldsymbol{\mu}_3'' & \mathbf{0} & \mathbf{0}\\ \mathbf{0} & \mathbf{0} & \mathbf{0} & -\widetilde{\mathbf{F}}^B\mathbf{R}_B^T & \mathbf{0} & -c_B\boldsymbol{\xi}_3'' & \mathbf{0}\\ \mathbf{0} & \mathbf{0} & \mathbf{0} & \mathbf{0} & \mathbf{0} & \mathbf{X}_B\boldsymbol{\xi}_3'' & \mathbf{0}\\ \mathbf{0} & \mathbf{0} & \mathbf{0} & \mathbf{0} & \mathbf{0} & \mathbf{0} & \mathbf{0}\\ \mathbf{0} & \mathbf{0} & \mathbf{0} & \mathbf{0} & \mathbf{0} & \mathbf{0} & \mathbf{0}\\ \mathbf{0} & \mathbf{0} & \mathbf{0} & \mathbf{0} & \mathbf{0} & \mathbf{0} & \mathbf{0}\end{bmatrix}$$

$$\mathbf{X}_A = \mathbf{R}_A^T(r_A\widetilde{\mathbf{F}}^A - c_A\widetilde{\mathbf{r}}_A) \qquad \mathbf{X}_B = \mathbf{R}_B^T(r_B\widetilde{\mathbf{F}}^B - c_B\widetilde{\mathbf{r}}_B)$$

$$\mathbf{S}_{q\lambda} = \begin{bmatrix} (\mathbf{F}^A/\lambda_1) & 0 & 0 \\ \mathbf{R}_A^T\tilde{\mathbf{r}}_A(\mathbf{F}^A/\lambda_1) & 0 & 0 \\ (\mathbf{F}^B/\lambda_1) & 0 & 0 \\ \mathbf{R}_B^T\tilde{\mathbf{r}}_B(\mathbf{F}^B/\lambda_1) & 0 & 0 \\ 0 & 0 & 0 \\ 0 & 0 & 0 \\ 0 & 0 & 0 \end{bmatrix} \tag{54}$$

$$\mathbf{S}_{\lambda q} = \mathbf{S}_{\lambda\lambda} = \mathbf{0}$$

## 7. Examples

The contributions of the gears-pair element are assembled to the rest of the mechanical system by following a standard procedure, leading to a system of differential/algebraic equations (DAE's). This system is in turn time integrated using the Hilber-Hughes-Taylor algorithm with an adaptive time step strategy (the whole procedure is described in [AM89, AM94]).

We present here three examples of application of the techniques for modeling gear pair systems. The two first ones concern kinematics analyses (i.e. zero mass is assumed) in which the variations of some degrees of freedom of the system are imposed to determine a new configuration. The resulting system of equations is solved using the Newton method at each step of the configurations sequence [SAM94, ACa89]. The third example is a dynamic analysis, where vibrations originated in gears error transmission are calculated. In this case, the equations of motion are numerically time integrated using the Hilber-Hughes-Taylor method.

### *7.1. Conical straight bevel pair*

The first example consists on a conical straight bevel gear pair, one wheel fixed and the other one mounted on a rigid bar which turns around the $y$-axis (figures 3,4).

The center of the first wheel is fixed at the coordinates origin. The wheel is lying in the $x - z$ plane. It has radius $r_A = 5$, normal modulus $m_n = 0.2$, pressure angle $\alpha_n = 20^o$, teeth number $z_A = 50$, cone angle $\gamma_A = -\tan^{-1}(5) = -78.7^o$ and helix angle $\beta_A = 0$. At the initial configuration, the second wheel has its center at $(0, 1, 5)$ and lies in a plane parallel to the $x-y$ plane. Its radius is $r_B = 1$, the teeth number $z_B = 10$, cone angle $\gamma_B = -\tan^{-1}(0.2) = -11.3^o$ and helix angle $\beta_B = 0$. It is hinged to a rigid bar which goes from $(0, 1, 5)$ to the point of coordinates $(0, 1, 0)$. At this point, the bar is connected through a hinge with axis along the $y$-axis to the foundation.

The system has one degree of freedom. A new configuration is found by imposing an incremental angle of 1 rad at the rigid bar. Also, a torque $M_{ext} = 1000$ is imposed at the articulation between the bar and the second wheel. Figure 3 displays the computed configuration together with the resulting

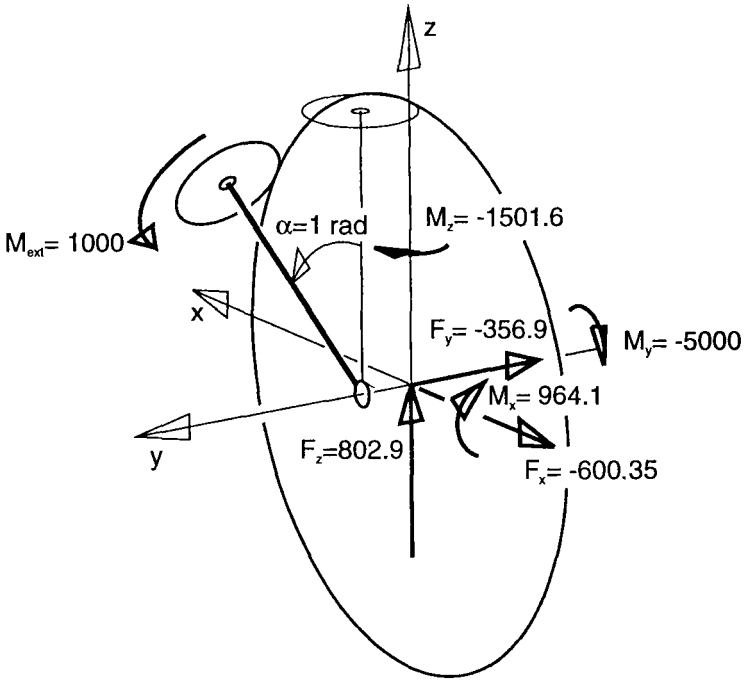


Figure 3: *Conical bevel pair*

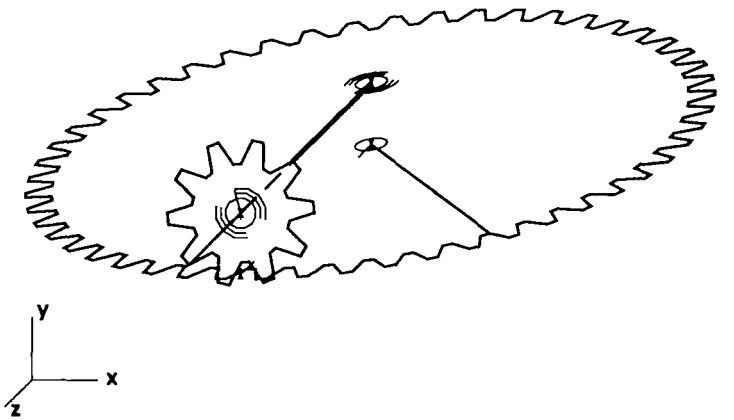


Figure 4: *Schematic view of conical bevel pair (program output)*

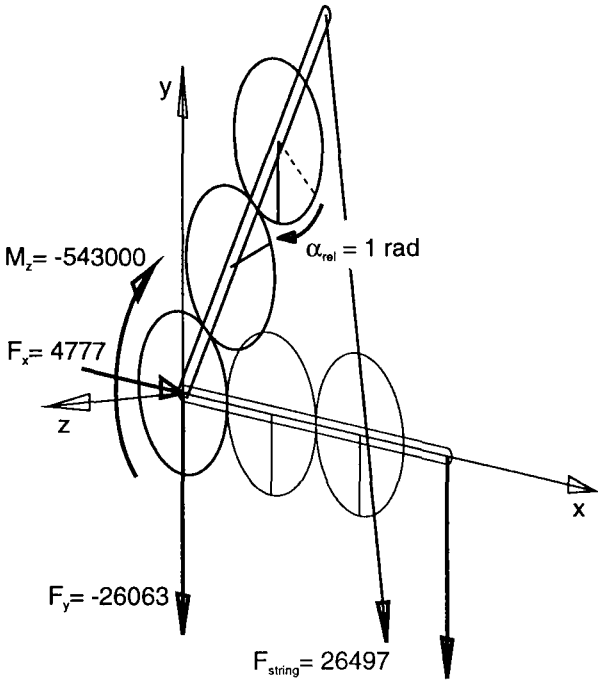


Figure 5: *Three-wheeled system*

actions of the first wheel upon the foundation. The computed normal contact force between gears was $F_{gear} = 1.064 \times 10^3$.

### *7.2. Three-wheeled system*

The second example consists on three equal spur gears mounted on a rigid bar (figures 5-6). The system is lying in the $x - y$ plane. The bar is articulated to the foundation at the coordinates origin. A string ($k_{string} = 1000, \quad l_0 = 50$) connects the extreme of the bar to the foundation at point $(30, -50, 0)$ (not shown in figure 5).

The three wheels have normal modulus $m_n = 0.2$, pitch diameter $d = 5$, pressure angle $\alpha_n = 20^o$ and teeth number $z = 50$ (clearly, the cone and helix angles are $\gamma = \beta = 0$). The first wheel –centered at the coordinates origin– is fixed to the foundation, while the rigid bar is articulated at the same point. The bar is aligned along the $x$-axis at the initial configuration.

The system is put in motion by imposing a relative angular displacement $\alpha_{rel} = 1$ rad at the third wheel, thus inducing a rotation of 1 rad of the bar about the origin as shown in figure 4. In the same figure we display the values of actions of the first wheel on the foundation for the new configuration, and also the value of force exerted by the string. The computed value of contact force between gears was $F_{gear} = 1.156 \times 10^5$.

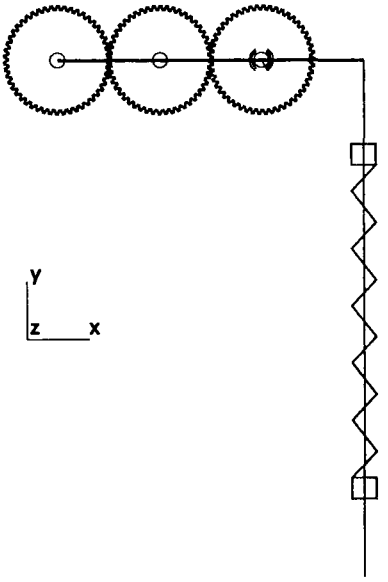


Figure 6: *Schematic view of the three-wheeled system (program output)*

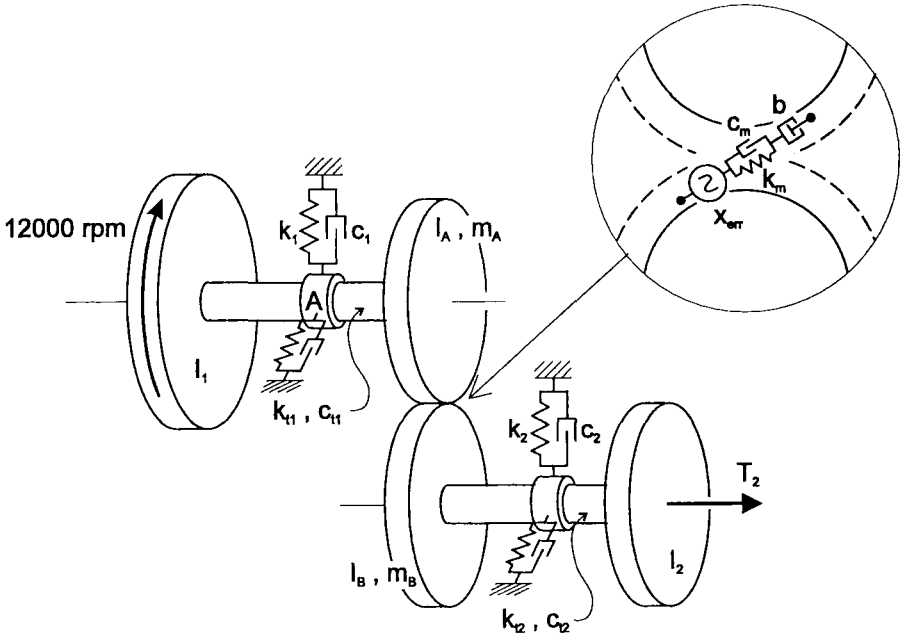


Figure 7: *Spur gears transmission*

### *7.3. Dynamic analysis of a spur gear transmission*

This example concerns the analysis of a transmission composed by two axes linked through a pair formed by two equal spur gears (see figure 7). This example corresponds to an experimental set-up made by Kubo et al [AKTS72], and was proposed also as test-case by Özgüven [HNO91] who estimated several system parameters of Kubo's work since some of them lacked in the paper. Most parameters we have used correspond to one of the analyses made by Özgüven. The only difference lies in the loaded error transmission expression. Our aim is just to show an example with approximate realistic data, illustrating about the possibilities of the code for making dynamic analyses of gear vibrations.

The system is driven at a constant speed of 12000 RPM at wheel 1, and transmits a torque $T_2 = 945.8$ applied at wheel 2. Gear properties are : normal modulus $m_n = 0.15748$, pitch diameter $d = 3.937$, pressure angle $\alpha_n = 20^o$ and teeth number $z_A = z_B = 25$ (cone and helix angles are trivially $\gamma = \beta = 0$). Their mass and rotary inertia are : $m_A = m_B = 5.36 \times 10^{-3}$ and $I_A = I_B = 0.0102$. Mesh stiffness is $k_m = 1.477 \times 10^7$, mesh damping $\xi = 0.1$, and the amplitude of the loaded transmission error is $X = 0.003937$ (equation (39)).

In accordance with the paper by Özgüven, we have considered only the torsional stiffness of shafts in the model, with values : $k_{t\,1} = 1.7 \times 10^4, k_{t\,2} = 3.0 \times 10^4$, and damping : $c_{t\,1} = 0.076026, c_{t\,2} = 0.12369$ (note that the program does not have any limitation in this sense and could have included other components of the axes deformation as well). Disks at extremes have rotary inertias $I_1 = 0.051$ and $I_2 = 0.0102$.

Four different conditions were analyzed, to illustrate the different kind of phenomena that can be observed when varying the model's characteristics :

A : Both axes are rigidly mounted at their supports, and backlash between gears is zero.

B : Horizontal and vertical flexibility of axes supports is considered, with stiffness values $k_1 = k_2 = 1.477 \times 10^7$ and damping $c_1 = c_2 = 50$. Backlash is zero.

C : The axes are rigidly supported, but backlash is introduced to the model, with value $b = 0.001968$.

D : This case incorporates both flexibility of supports and backlash to the model. Numerical values are equal to those mentioned in cases B and C.

An *almost* stationary system response is evidenced from results. To this end, we have time integrated the system equations up to a time instant in which all initial transients seemed to be damped-out. In order to reach quickly the stationary phase, we have performed the following computation steps : first, we evaluated the static deformation under the action of torque $T_2$; secondly, we made a kinematics analysis in which the system was put into motion at 12000 RPM, by ignoring all inertial forces and starting from the deformed configuration computed at the first phase; finally, a full transient analysis was performed,

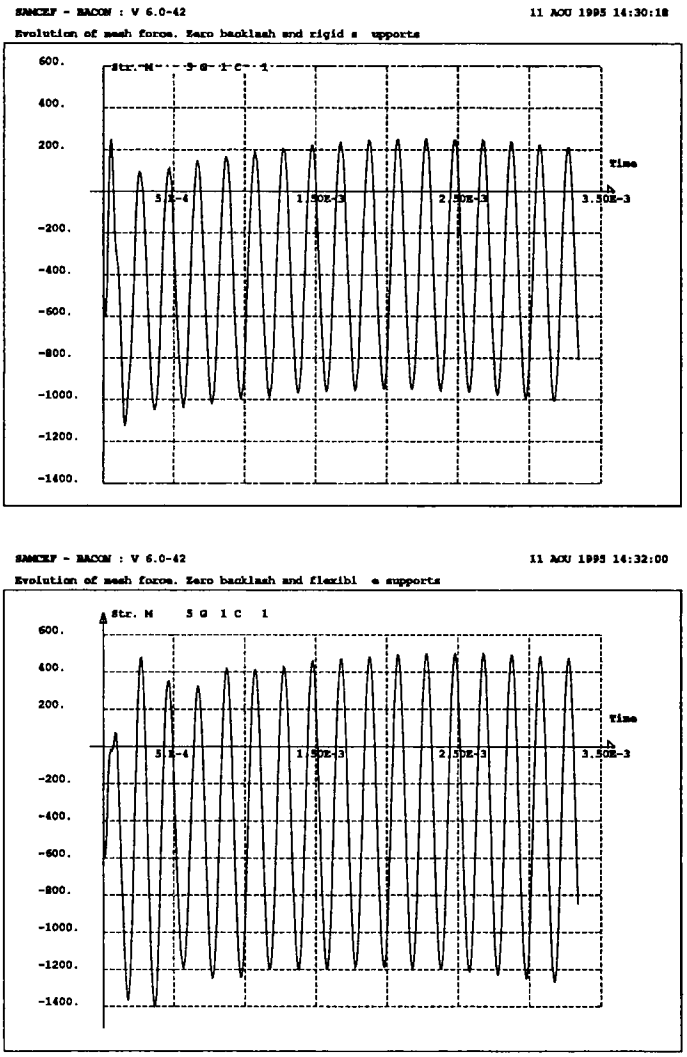


Figure 8: *Spur gears transmission : time evolution of mesh force. Analysis without considering backlash. Top : rigid supports case (A); bottom : flexible supports case (B).*

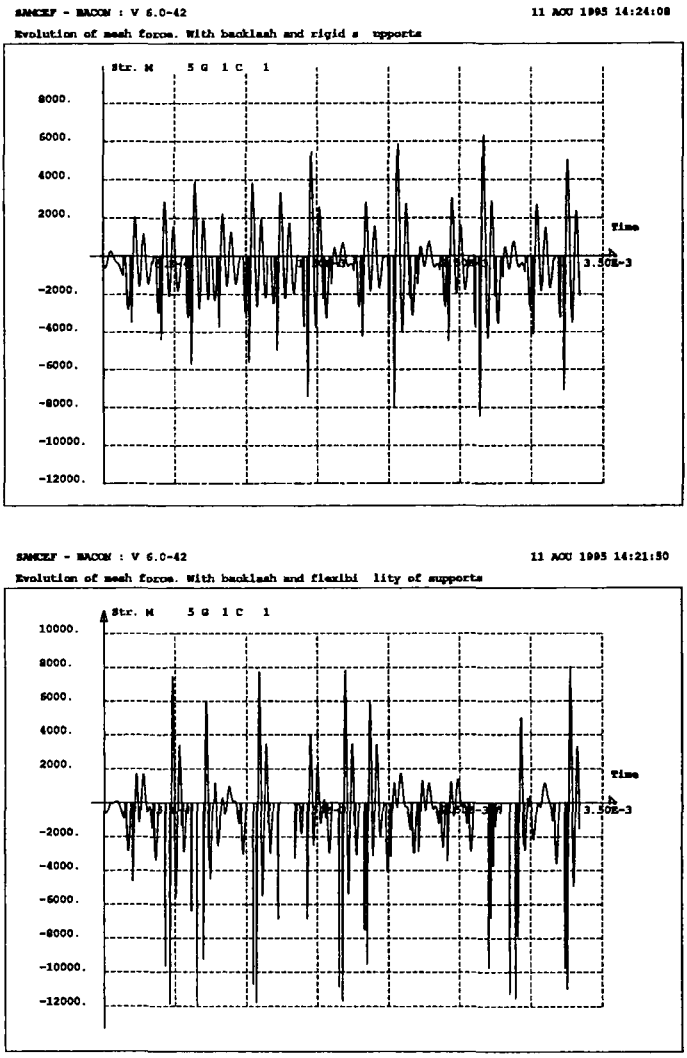


Figure 9: *Spur gears transmission : time evolution of mesh force. Analysis including backlash. Top : rigid supports case (C); bottom : flexible supports case (D).*

starting from the configuration and velocities computed at the previous phase of analysis.

Figures 8 and 9 display the time evolution of the total mesh force for the four cases. In all cases, after initial transients are damped-out, a quasi-periodic response is obtained as expected. We can also appreciate the effects of supports flexibility and backlash :

- The inclusion of supports flexibility does not affect sensibly the frequency content of the response. However, the force amplitude of oscillation is increased by a factor of 1.4.
- When backlash is included into the model, the frequency content of the mesh force is increased by a factor of almost 4. Also note that the force amplitude increases by a factor nearly equal to 15.

Figures 10 and 11 show the time evolution of the horizontal reaction at support A. Results evidence approximately the same overall behavior as that of the teeth force; nevertheless, the following special features can be remarked :

- In the zero-backlash case, and when considering supports flexibility, the horizontal reaction is magnified by a factor of almost 2, instead of the factor 1.5 evidenced for the mesh force (figure 10).
- Contrary to what has happened with the mesh forces evolution, the amplitude of horizontal reactions in the flexible supports case is lower than that of the rigid supports one (figure 11).

Figures 12 and 13 plot the time evolution of the vertical reaction at support A. We note now the system behavior does not follow that of the mesh force evolution shown in figures 8 and 9. The following remarks can be made for the evolution of this component of the reaction force :

- We note that in the rigid supports case, the reaction force is negative for all time instants, in accordance with the special nature of contact between gears. Positive reaction forces are only developed when flexibility of supports is taken into account.
- The case with rigid supports and backlash evidences a much higher frequency content than the other three analyses. The amplitude of force oscillations verifies approximately the same relationships as those discussed in the horizontal reactions analysis.

Although the particular values of mesh and support stiffness and damping did not correspond fully to the experimental setup, we understand this example serves to illustrate the kind of phenomena we can expect when analyzing vibrations in gear trains and the potential of the approach presented in the paper.

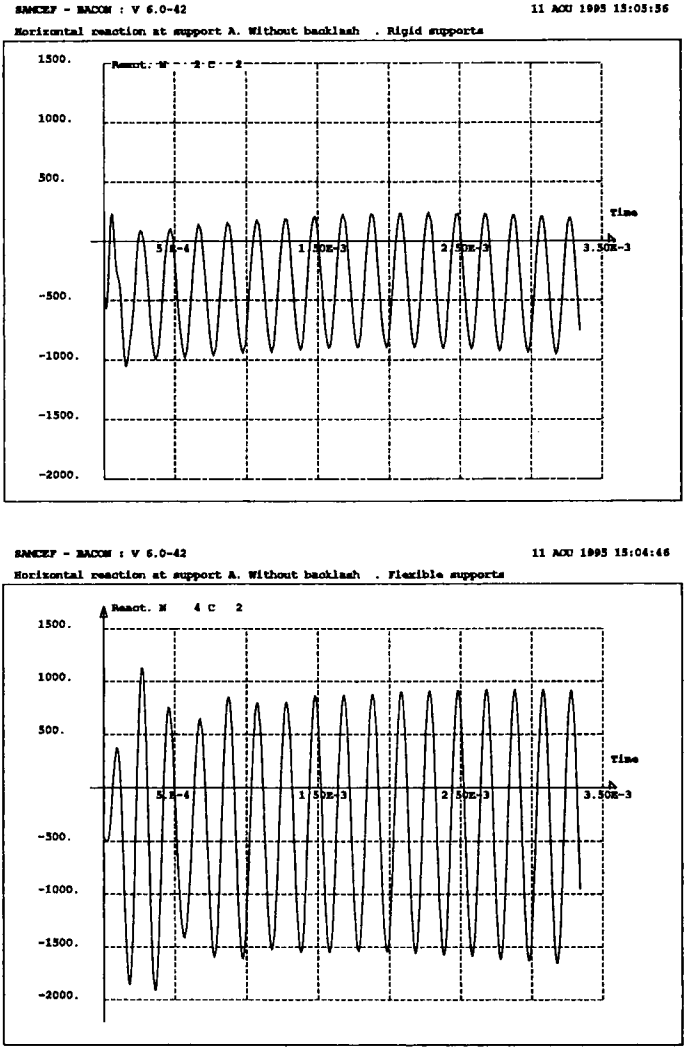


Figure 10: *Spur gears transmission : time evolution of horizontal reaction at support A. Analysis without considering backlash. Top : rigid supports case (A); bottom : flexible supports case (B).*

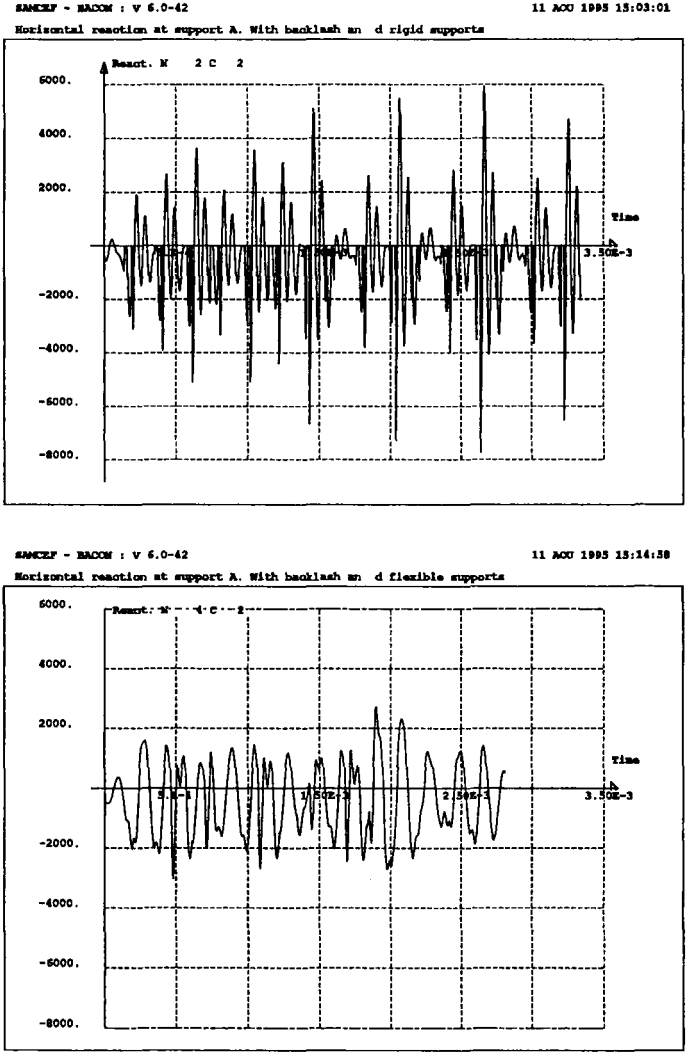


Figure 11: *Spur gears transmission : time evolution of horizontal reaction at support A. Analysis including backlash. Top : rigid supports case (C); bottom : flexible supports case (D).*

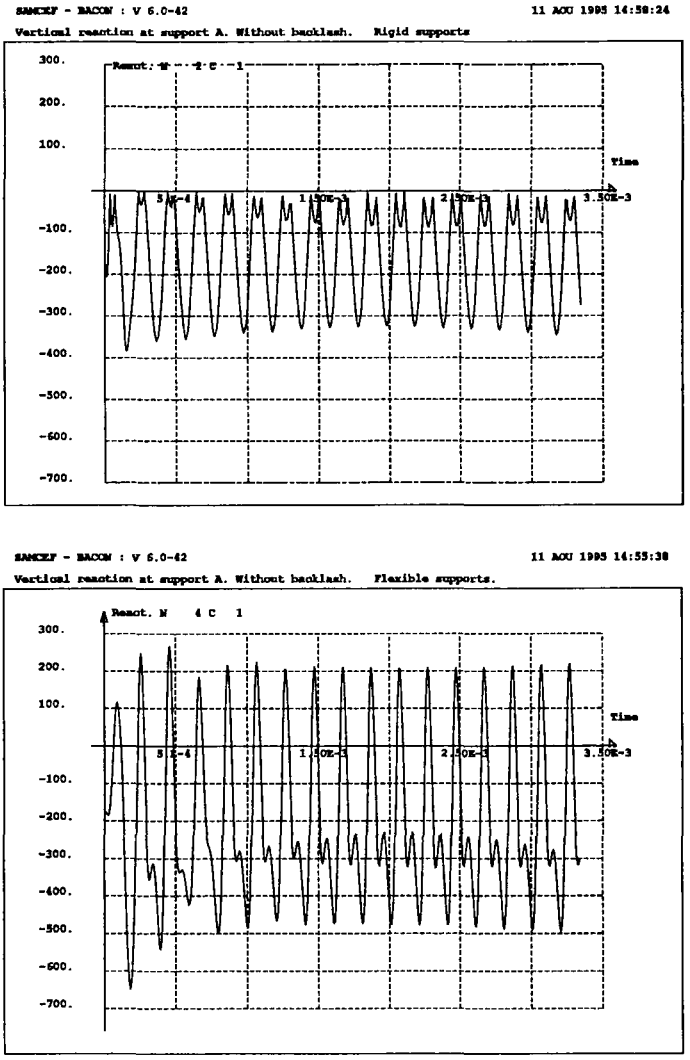


Figure 12: *Spur gears transmission : time evolution of vertical reaction at support A. Analysis without considering backlash. Top : rigid supports case (A); bottom : flexible supports case (B).*

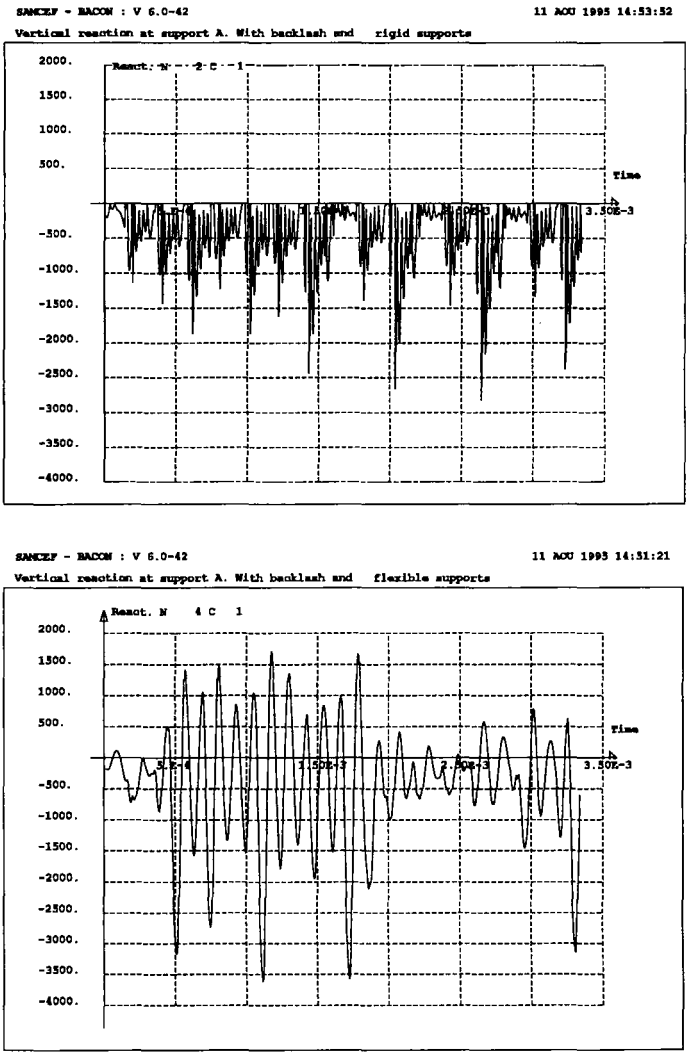


Figure 13: *Spur gears transmission : time evolution of vertical reaction at support A. Analysis including backlash. Top : rigid supports case (C); bottom : flexible supports case (D).*

## 8. Concluding remarks

A general methodology to formulate gear pair connections in three-dimensional kinematics and dynamic analysis of mechanisms has been proposed. Holonomic constraint equations were generated by using an augmented Lagrangian technique, while non-holonomic radial and friction forces were explicitly added to the Euler-Lagrange equations of the dynamic system. Gear teeth flexibility was taken into account in the model by relating deformation along the normal pressure line to the normal forces acting on teeth.

The joint discussed here forms part of the vast library of joints of the multiple purpose software for mechanism analysis *Mecano* (see [SAM94] for a detailed description of this library), and adds new functionalities to the code. The capability of modeling three dimensional gears together with the rest of (flexible and rigid) joints and bodies of the code results in a very valuable tool for the design of mechanisms and machines.

Three examples of application have been shown. Mechanisms including conical straight bevel pairs, three spur-geared wheels and a system composed by two axes connected through a spur gear pair have been analyzed, illustrating the generality of the formulation. The latter example included the effects of teeth flexibility, stiffness fluctuation and backlash in the analysis, allowing to compute system vibrations originated by the fluctuations of stiffness and other transmission errors.

### Acknowledgements

This work received financial support from *Conicet* through grant PID-BID 238 and from *Fundación Antorchas* through grant A-13218/1-10.

### References

[ACa89] A.Cardona. *An Integrated Approach to Mechanism Analysis.* PhD thesis, Université de Liège, Belgium, 1989. Collection des Publications de la Faculté des Sciences Appliquées 127.

[ACa95] A.Cardona. Three dimensional gears modeling in multibody systems analysis. 1995. submitted to International Journal for Numerical Methods in Engineering.

[AKa94a] A.Kahraman. Load sharing characteristics of planetary transmissions. *Mech. Mach. Theory*, 29:1151–1165, 1994.

[AKa94b] A.Kahraman. Planetary gear train dynamics. *Journal of Mechanical Design*, 116:713–720, 1994.

[AKTS72] A.Kubo, K.Yamada, T.Aida, and S.Sato. Research on ultra speed gear devices (reports 1-3). *Transactions of the Japan Society of Mechanical Engineers*, 38:2692–2715, 1972.

[AM88] A.Cardona and M.Géradin. A beam finite element nonlinear theory with finite rotations. *Int. J. Num. Meth. Engng.*, 26:2403–2438, 1988.

[AM89] A.Cardona and M.Géradin. Time integration of the equations of motion in mechanism analysis. *Comput. & Structures*, 33:801–820, 1989.

[AM94] A.Cardona and M.Géradin. Numerical integration of second order differential - algebraic systems in flexible mechanism dynamics. *NATO ASI Series*, 268:501–529, 1994. Computer - Aided Analysis of Rigid and Flexible Mechanical Systems, ed. by M.F.O.Seabra Pereira and J.A.C.Ambrósio, Kluwer.

[AMD91] A.Cardona, M.Géradin, and D.B.Doan. Rigid and flexible joint modeling in multibody dynamics using finite elements. *Comput. Methods Appl. Mech. Engrg.*, 89:395–418, 1991.

[DA89] D.Z.Xiao and A.T.Yang. Kinematics of three dimensional gearing. *Mech. Mach. Theory*, 24:245–255, 1989.

[HD88a] H.N.Özgüven and D.R.Houser. Dynamic analysis of high speed gears by using loaded static transmission error. *J.Sound Vibration*, 125:71–83, 1988.

[HD88b] H.N.Özgüven and D.R.Houser. Mathematical models used in gear dynamics – a review. *J.Sound Vibration*, 121:383–411, 1988.

[HNO91] H.N.Özgüven. A non-linear mathematical model for dynamic analysis of spur gears including shaft and bearing dynamics. *J.Sound Vibration*, 145:239–260, 1991.

[JJ80] J.E.Shigley and J.J.Uicker Jr. *Theory of Machines and Mechanisms.* Mc Graw-Hill, New York, 1980.

[MD86] M.Tavakoli and D.R.Houser. Optimum profile modification for the minimization of static transmission errors of spur gears. *Journal of Mechanisms, Power, Transmissions, and Automation in Design, Transactions of the ASME*, 108:86–94, 1986.

[MG81] M.Géradin and G.Robert. *Vibrations de Torsion et de Flexion d'un Train d'Engrenages.* LTAS-Rapport VF-42, Université de Liège, Belgium, 1981.

[RG93] C.Rama Mohana Rao and G.Muthuveerappan. Finite element modeling and stress analysis of helical gear teeth. *Comp. & Struct.*, 49:1095–1106, 1993.

[SAM94] *SAMCEF – Module d'Analyse de Mécanismes MECANO (Manuel d'Utilisation).* 1994.

[SH93] Ö.S. Sener and H.N.Özgüven. Dynamic analysis of geared shaft systems by using a continuous system model. *J.Sound Vibration*, 166:539–556, 1993.